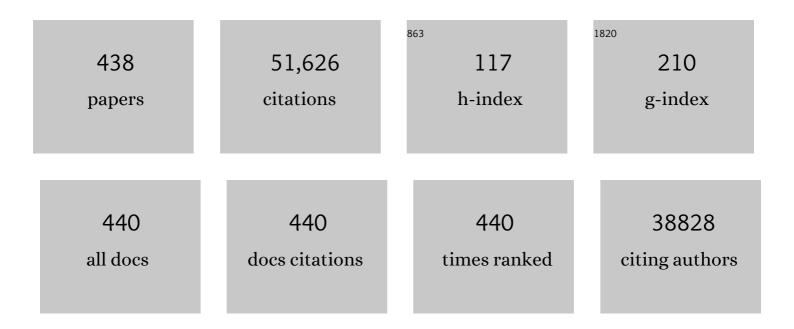
Chongmin Wang

List of Publications by Year in descending order

Source: https://exaly.com/author-pdf/8773319/publications.pdf Version: 2024-02-01



#	Article	IF	CITATIONS
1	Atomistic observation on diffusion-mediated friction between single-asperity contacts. Nature Materials, 2022, 21, 173-180.	13.3	16
2	Nonsacrificial Additive for Tuning the Cathode–Electrolyte Interphase of Lithium-Ion Batteries. ACS Applied Materials & Interfaces, 2022, 14, 4111-4118.	4.0	8
3	Locking oxygen in lattice: A quantifiable comparison of gas generation in polycrystalline and single crystal Ni-rich cathodes. Energy Storage Materials, 2022, 47, 195-202.	9.5	50
4	Fluorinationâ€Enhanced Surface Stability of Disordered Rocksalt Cathodes. Advanced Materials, 2022, 34, e2106256.	11.1	11
5	Assessing Longâ€Term Cycling Stability of Singleâ€Crystal Versus Polycrystalline Nickelâ€Rich NCM in Pouch Cells with 6 mAh cm ^{â^2} Electrodes. Small, 2022, 18, e2107357.	5.2	41
6	Stacking Faults Assist Lithium-Ion Conduction in a Halide-Based Superionic Conductor. Journal of the American Chemical Society, 2022, 144, 5795-5811.	6.6	50
7	Sulfone-based electrolytes for high energy density lithium-ion batteries. Journal of Power Sources, 2022, 527, 231171.	4.0	21
8	Facile Dual-Protection Layer and Advanced Electrolyte Enhancing Performances of Cobalt-free/Nickel-rich Cathodes in Lithium-Ion Batteries. ACS Applied Materials & Interfaces, 2022, 14, 17405-17414.	4.0	8
9	Nanotwin assisted reversible formation of low angle grain boundary upon reciprocating shear load. Acta Materialia, 2022, 230, 117850.	3.8	8
10	Interfacial-engineering-enabled practical low-temperature sodium metal battery. Nature Nanotechnology, 2022, 17, 269-277.	15.6	69
11	<i>In-situ</i> observation of deformation twin associated sub-grain boundary formation in copper single crystal under bending. Materials Research Letters, 2022, 10, 488-495.	4.1	5
12	Amine-Wetting-Enabled Dendrite-Free Potassium Metal Anode. ACS Nano, 2022, 16, 7291-7300.	7.3	36
13	Early Failure of Lithium–Sulfur Batteries at Practical Conditions: Crosstalk between Sulfur Cathode and Lithium Anode. Advanced Science, 2022, 9, e2201640.	5.6	12
14	Dual Protective Mechanism of AlPO ₄ Coating on High-Nickel Cathode Material for High Energy Density and Long Cycle Life Lithium-Ion Batteries. Journal of the Electrochemical Society, 2022, 169, 050523.	1.3	4
15	Improving LiNiO ₂ cathode performance through particle design and optimization. Journal of Materials Chemistry A, 2022, 10, 12890-12899.	5.2	16
16	Exceptional Cycling Performance Enabled by Local Structural Rearrangements in Disordered Rocksalt Cathodes. Advanced Energy Materials, 2022, 12, .	10.2	15
17	Review of recent progress on in situ TEM shear deformation: a retrospective and perspective view. Journal of Materials Science, 2022, 57, 12177-12201.	1.7	6
18	Low-solvation electrolytes for high-voltage sodium-ion batteries. Nature Energy, 2022, 7, 718-725.	19.8	137

#	Article	IF	CITATIONS
19	A Lithium Feedstock Pathway: Coupled Electrochemical Extraction and Direct Battery Materials Manufacturing. ACS Energy Letters, 2022, 7, 2420-2427.	8.8	9
20	Mesoscale-architecture-based crack evolution dictating cycling stability of advanced lithium ion batteries. Nano Energy, 2021, 79, 105420.	8.2	36
21	Optimization of fluorinated orthoformate based electrolytes for practical high-voltage lithium metal batteries. Energy Storage Materials, 2021, 34, 76-84.	9.5	65
22	Rational Design of Electrolytes for Long-Term Cycling of Si Anodes over a Wide Temperature Range. ACS Energy Letters, 2021, 6, 387-394.	8.8	58
23	All solid thick oxide cathodes based on low temperature sintering for high energy solid batteries. Energy and Environmental Science, 2021, 14, 5044-5056.	15.6	41
24	Strategies towards enabling lithium metal in batteries: interphases and electrodes. Energy and Environmental Science, 2021, 14, 5289-5314.	15.6	156
25	Effects of fluorinated solvents on electrolyte solvation structures and electrode/electrolyte interphases for lithium metal batteries. Proceedings of the National Academy of Sciences of the United States of America, 2021, 118, .	3.3	131
26	Electrolyte Regulating toward Stabilization of Cobalt-Free Ultrahigh-Nickel Layered Oxide Cathode in Lithium-Ion Batteries. ACS Energy Letters, 2021, 6, 1324-1332.	8.8	53
27	Fluorinationâ€Enhanced Surface Stability of Cationâ€Disordered Rocksalt Cathodes for Liâ€lon Batteries. Advanced Functional Materials, 2021, 31, 2101888.	7.8	28
28	Advanced Lowâ€Flammable Electrolytes for Stable Operation of Highâ€Voltage Lithiumâ€Ion Batteries. Angewandte Chemie, 2021, 133, 13109-13116.	1.6	16
29	Advanced Lowâ€Flammable Electrolytes for Stable Operation of Highâ€Voltage Lithiumâ€Ion Batteries. Angewandte Chemie - International Edition, 2021, 60, 12999-13006.	7.2	70
30	Stabilizing ultrahigh-nickel layered oxide cathodes for high-voltage lithium metal batteries. Materials Today, 2021, 44, 15-24.	8.3	53
31	Origin, Nature, and the Dynamic Behavior of Nanoscale Vacancy Clusters in Ni-Rich Layered Oxide Cathodes. ACS Applied Materials & Interfaces, 2021, 13, 18849-18855.	4.0	7
32	Electrochemical scissoring of disordered silicon-carbon composites for high-performance lithium storage. Energy Storage Materials, 2021, 36, 139-146.	9.5	20
33	Polymer-ceramic composite electrolytes for all-solid-state lithium batteries: Ionic conductivity and chemical interaction enhanced by oxygen vacancy in ceramic nanofibers. Journal of Power Sources, 2021, 495, 229796.	4.0	40
34	Optimization of Magnesiumâ€Doped Lithium Metal Anode for High Performance Lithium Metal Batteries through Modeling and Experiment. Angewandte Chemie, 2021, 133, 16642-16649.	1.6	5
35	Balancing interfacial reactions to achieve long cycle life in high-energy lithium metal batteries. Nature Energy, 2021, 6, 723-732.	19.8	285
36	Optimization of Magnesiumâ€Doped Lithium Metal Anode for High Performance Lithium Metal Batteries through Modeling and Experiment. Angewandte Chemie - International Edition, 2021, 60, 16506-16513.	7.2	28

#	Article	IF	CITATIONS
37	A Polymer-in-Salt Electrolyte with Enhanced Oxidative Stability for Lithium Metal Polymer Batteries. ACS Applied Materials & Interfaces, 2021, 13, 31583-31593.	4.0	28
38	In-Situ Environmental TEM Study of Solid-Gas Interfacial Process in Energy Materials. Microscopy and Microanalysis, 2021, 27, 1970-1971.	0.2	0
39	In-situ TEM observation of bending induced sub-grain boundary formation in copper single crystal. Microscopy and Microanalysis, 2021, 27, 3414-3415.	0.2	0
40	Progressive growth of the solid–electrolyte interphase towards the Si anode interior causes capacity fading. Nature Nanotechnology, 2021, 16, 1113-1120.	15.6	147
41	Formation of LiF Surface Layer During Direct Fluorination of High-Capacity Co-Free Disordered Rocksalt Cathodes. ACS Applied Materials & amp; Interfaces, 2021, 13, 38221-38228.	4.0	13
42	The passivity of lithium electrodes in liquid electrolytes for secondary batteries. Nature Reviews Materials, 2021, 6, 1036-1052.	23.3	201
43	Interplay between Cation and Anion Redox in Ni-Based Disordered Rocksalt Cathodes. ACS Nano, 2021, 15, 13360-13369.	7.3	13
44	A Micrometer‣ized Silicon/Carbon Composite Anode Synthesized by Impregnation of Petroleum Pitch in Nanoporous Silicon. Advanced Materials, 2021, 33, e2103095.	11.1	99
45	Role of Fluorine in Chemomechanics of Cation-Disordered Rocksalt Cathodes. Chemistry of Materials, 2021, 33, 7028-7038.	3.2	8
46	Stable Solid Electrolyte Interphase Layer Formed by Electrochemical Pretreatment of Gel Polymer Coating on Li Metal Anode for Lithium–Oxygen Batteries. ACS Energy Letters, 2021, 6, 3321-3331.	8.8	17
47	Labile Fe(III) supersaturation controls nucleation and properties of product phases from Fe(II)-catalyzed ferrihydrite transformation. Geochimica Et Cosmochimica Acta, 2021, 309, 272-285.	1.6	24
48	Toward the Practical Use of Cobalt-Free Lithium-Ion Batteries by an Advanced Ether-Based Electrolyte. ACS Applied Materials & Interfaces, 2021, 13, 44339-44347.	4.0	24
49	Atomistic processes of surface-diffusion-induced abnormal softening in nanoscale metallic crystals. Nature Communications, 2021, 12, 5237.	5.8	27
50	Exposure History and its Effect Towards Stabilizing Li Exchange Across Disordered Rock Salt Interfaces. ChemElectroChem, 2021, 8, 3982-3991.	1.7	4
51	In-situ TEM observation of shear induced microstructure evolution in Cu-Nb alloy. Scripta Materialia, 2021, 205, 114214.	2.6	6
52	LT-LiMn _{0.5} Ni _{0.5} O ₂ : a unique co-free cathode for high energy Li-ion cells. Chemical Communications, 2021, 57, 11009-11012.	2.2	8
53	Recent Progress in Understanding Solid Electrolyte Interphase on Lithium Metal Anodes. Advanced Energy Materials, 2021, 11, 2003092.	10.2	271
54	Compact Sn/SnO2 microspheres with gradient composition for high volumetric lithium storage. Energy Storage Materials, 2020, 25, 376-381.	9.5	27

#	Article	IF	CITATIONS
55	Labile Fe(III) from sorbed Fe(II) oxidation is the key intermediate in Fe(II)-catalyzed ferrihydrite transformation. Geochimica Et Cosmochimica Acta, 2020, 272, 105-120.	1.6	72
56	Atomic to Nanoscale Origin of Vinylene Carbonate Enhanced Cycling Stability of Lithium Metal Anode Revealed by Cryo-Transmission Electron Microscopy. Nano Letters, 2020, 20, 418-425.	4.5	102
57	Realâ€Time Atomicâ€Scale Visualization of Reversible Copper Surface Activation during the CO Oxidation Reaction. Angewandte Chemie - International Edition, 2020, 59, 2505-2509.	7.2	24
58	Realâ€Time Atomicâ€Scale Visualization of Reversible Copper Surface Activation during the CO Oxidation Reaction. Angewandte Chemie, 2020, 132, 2526-2530.	1.6	11
59	Reversible Electrochemical Interface of Mg Metal and Conventional Electrolyte Enabled by Intermediate Adsorption. ACS Energy Letters, 2020, 5, 200-206.	8.8	44
60	Atomic-Scale Dynamic Interaction of <mml:math <br="" xmlns:mml="http://www.w3.org/1998/Math/MathML">display="inline"><mml:mrow><mml:msub><mml:mrow><mml:mi mathvariant="normal">H</mml:mi </mml:mrow><mml:mrow><mml:mn>2</mml:mn></mml:mrow></mml:msub> mathvariant="normal">O</mml:mrow></mml:math> Molecules with Cu Surface. Physical Review Letters, 2020, 125, 156101.	> Ձıŋ ml:mi	11
61	Unravelling high-temperature stability of lithium-ion battery with lithium-rich oxide cathode in localized high-concentration electrolyte. Journal of Power Sources Advances, 2020, 5, 100024.	2.6	23
62	New synthesis strategies to improve Co-Free LiNi0.5Mn0.5O2 cathodes: Early transition metal d0 dopants and manganese pyrophosphate coating. Journal of Power Sources, 2020, 479, 228591.	4.0	22
63	Controlling Ion Coordination Structure and Diffusion Kinetics for Optimized Electrode-Electrolyte Interphases and High-Performance Si Anodes. Chemistry of Materials, 2020, 32, 8956-8964.	3.2	24
64	Electrolyte-Phobic Surface for the Next-Generation Nanostructured Battery Electrodes. Nano Letters, 2020, 20, 7455-7462.	4.5	25
65	Understanding Reactivities of Ni-Rich Li[Ni _{<i>x</i>} Mn _{<i>y</i>} Co _{1–<i>x</i>–<i>y</i>}]O ₂ Single-Crystal Cathode Materials. ACS Applied Energy Materials, 2020, 3, 12238-12245.	2.5	24
66	Enabling Ether-Based Electrolytes for Long Cycle Life of Lithium-Ion Batteries at High Charge Voltage. ACS Applied Materials & Interfaces, 2020, 12, 54893-54903.	4.0	35
67	Direct Contacting with Liquid Electrolyte Facilitates the Surface Phase Transition in Ni-rich Layered Cathode. Microscopy and Microanalysis, 2020, 26, 3018-3020.	0.2	2
68	Ultra-Microtome for the Preparation of TEM Specimens from Battery Cathodes. Microscopy and Microanalysis, 2020, 26, 867-877.	0.2	9
69	Highly Reversible Sodium Ion Batteries Enabled by Stable Electrolyte-Electrode Interphases. ACS Energy Letters, 2020, 5, 3212-3220.	8.8	97
70	<i>In situ</i> electrochemical scanning/transmission electron microscopy of electrode–electrolyte interfaces. MRS Bulletin, 2020, 45, 738-745.	1.7	19
71	In-situ TEM Coupled with AFM Cantilever for Direct Observation of Li Dendrite Nucleation and Growth Under Stress. Microscopy and Microanalysis, 2020, 26, 3038-3039.	0.2	0
72	Reversible planar gliding and microcracking in a single-crystalline Ni-rich cathode. Science, 2020, 370, 1313-1317.	6.0	472

#	Article	IF	CITATIONS
73	Hidden Subsurface Reconstruction and Its Atomic Origins in Layered Oxide Cathodes. Microscopy and Microanalysis, 2020, 26, 2542-2544.	0.2	Ο
74	Role of inner solvation sheath within salt–solvent complexes in tailoring electrode/electrolyte interphases for lithium metal batteries. Proceedings of the National Academy of Sciences of the United States of America, 2020, 117, 28603-28613.	3.3	191
75	Designing Advanced In Situ Electrode/Electrolyte Interphases for Wide Temperature Operation of 4.5 V Li LiCoO ₂ Batteries. Advanced Materials, 2020, 32, e2004898.	11.1	123
76	Redox Behaviors in a Li-Excess Cation-Disordered Mn–Nb–O–F Rocksalt Cathode. Chemistry of Materials, 2020, 32, 4490-4498.	3.2	37
77	Direct observation of dual-step twinning nucleation in hexagonal close-packed crystals. Nature Communications, 2020, 11, 2483.	5.8	59
78	Unstable twin in body-centered cubic tungsten nanocrystals. Nature Communications, 2020, 11, 2497.	5.8	40
79	Sweeping potential regulated structural and chemical evolution of solid-electrolyte interphase on Cu and Li as revealed by cryo-TEM. Nano Energy, 2020, 76, 105040.	8.2	16
80	Vacancy ordering during selective oxidation of \hat{I}^2 -NiAl. Materialia, 2020, 12, 100783.	1.3	6
81	Hierarchical porous silicon structures with extraordinary mechanical strength as high-performance lithium-ion battery anodes. Nature Communications, 2020, 11, 1474.	5.8	298
82	Optimized Al Doping Improves Both Interphase Stability and Bulk Structural Integrity of Ni-Rich NMC Cathode Materials. ACS Applied Energy Materials, 2020, 3, 3369-3377.	2.5	66
83	The Role of Secondary Particle Structures in Surface Phase Transitions of Ni-Rich Cathodes. Chemistry of Materials, 2020, 32, 2884-2892.	3.2	60
84	Tin-graphene tubes as anodes for lithium-ion batteries with high volumetric and gravimetric energy densities. Nature Communications, 2020, 11, 1374.	5.8	127
85	Current Density Regulated Atomic to Nanoscale Process on Li Deposition and Solid Electrolyte Interphase Revealed by Cryogenic Transmission Electron Microscopy. ACS Nano, 2020, 14, 8766-8775.	7.3	54
86	Unlocking the passivation nature of the cathode–air interfacial reactions in lithium ion batteries. Nature Communications, 2020, 11, 3204.	5.8	55
87	Evolution of the rate-limiting step: From thin film to thick Ni-rich cathodes. Journal of Power Sources, 2020, 454, 227966.	4.0	35
88	Hidden Subsurface Reconstruction and Its Atomic Origins in Layered Oxide Cathodes. Nano Letters, 2020, 20, 2756-2762.	4.5	24
89	Ligninâ€derived electrochemical energy materials and systems. Biofuels, Bioproducts and Biorefining, 2020, 14, 650-672.	1.9	73
90	Real-time mass spectrometric characterization of the solid–electrolyte interphase of a lithium-ion battery. Nature Nanotechnology, 2020, 15, 224-230.	15.6	280

#	Article	IF	CITATIONS
91	Dynamic Atom Clusters on AuCu Nanoparticle Surface during CO Oxidation. Journal of the American Chemical Society, 2020, 142, 4022-4027.	6.6	36
92	Controlling Surface Phase Transition and Chemical Reactivity of O3-Layered Metal Oxide Cathodes for High-Performance Na-Ion Batteries. ACS Energy Letters, 2020, 5, 1718-1725.	8.8	64
93	Deciphering atomistic mechanisms of the gas-solid interfacial reaction during alloy oxidation. Science Advances, 2020, 6, eaay8491.	4.7	20
94	Advances in metal–organic framework coatings: versatile synthesis and broad applications. Chemical Society Reviews, 2020, 49, 3142-3186.	18.7	327
95	Excellent Cycling Stability of Sodium Anode Enabled by a Stable Solid Electrolyte Interphase Formed in Etherâ€Based Electrolytes. Advanced Functional Materials, 2020, 30, 2001151.	7.8	60
96	Electrolyte design for LiF-rich solid–electrolyte interfaces to enable high-performance microsized alloy anodes for batteries. Nature Energy, 2020, 5, 386-397.	19.8	621
97	Advanced Electrolytes for Fastâ€Charging Highâ€Voltage Lithiumâ€Ion Batteries in Wideâ€Temperature Range. Advanced Energy Materials, 2020, 10, 2000368.	10.2	159
98	Electrocatalytic Hydrogen Evolution in Neutral pH Solutions: Dual-Phase Synergy. ACS Catalysis, 2019, 9, 8712-8718.	5.5	103
99	High temperature shockwave stabilized single atoms. Nature Nanotechnology, 2019, 14, 851-857.	15.6	278
100	Lattice doping regulated interfacial reactions in cathode for enhanced cycling stability. Nature Communications, 2019, 10, 3447.	5.8	116
101	Highâ€Performance Silicon Anodes Enabled By Nonflammable Localized Highâ€Concentration Electrolytes. Advanced Energy Materials, 2019, 9, 1900784.	10.2	175
102	Enabling High-Voltage Lithium-Metal Batteries under Practical Conditions. Joule, 2019, 3, 1662-1676.	11.7	598
103	Polymerâ€inâ€â€œQuasiâ€ionic Liquid―Electrolytes for Highâ€Voltage Lithium Metal Batteries. Advanced Energ Materials, 2019, 9, 1902108.	gy _{10.2}	65
104	Origin of lithium whisker formation and growth under stress. Nature Nanotechnology, 2019, 14, 1042-1047.	15.6	211
105	In-situ S/TEM Probing of the Coupling among Electrochemical, Thermal, and Mechanical Effect in Rechargeable Batteries. Microscopy and Microanalysis, 2019, 25, 2164-2165.	0.2	0
106	A high-performance oxygen evolution catalyst in neutral-pH for sunlight-driven CO2 reduction. Nature Communications, 2019, 10, 4081.	5.8	57
107	Monolithic solid–electrolyte interphases formed in fluorinated orthoformate-based electrolytes minimize Li depletion and pulverization. Nature Energy, 2019, 4, 796-805.	19.8	621
108	Nonflammable Electrolytes for Lithium Ion Batteries Enabled by Ultraconformal Passivation Interphases. ACS Energy Letters, 2019, 4, 2529-2534.	8.8	112

#	Article	IF	CITATIONS
109	Atomic-Scale Mechanisms of Enhanced Electrochemical Properties of Mo-Doped Co-Free Layered Oxide Cathodes for Lithium-Ion Batteries. ACS Energy Letters, 2019, 4, 2540-2546.	8.8	40
110	Building advanced materials via particle aggregation and molecular self-assembly. Journal of Materials Research, 2019, 34, 2911-2913.	1.2	0
111	In Situ Transmission Electron Microscopy Studies of Electrochemical Reaction Mechanisms in Rechargeable Batteries. Electrochemical Energy Reviews, 2019, 2, 467-491.	13.1	30
112	Ni/Li Disordering in Layered Transition Metal Oxide: Electrochemical Impact, Origin, and Control. Accounts of Chemical Research, 2019, 52, 2201-2209.	7.6	315
113	Infinitesimal sulfur fusion yields quasi-metallic bulk silicon for stable and fast energy storage. Nature Communications, 2019, 10, 2351.	5.8	57
114	Atomic-scale combination of germanium-zinc nanofibers for structural and electrochemical evolution. Nature Communications, 2019, 10, 2364.	5.8	44
115	Interconnected Vertically Stacked 2D-MoS ₂ for Ultrastable Cycling of Rechargeable Li-Ion Battery. ACS Applied Materials & Interfaces, 2019, 11, 20762-20769.	4.0	37
116	Constructing Robust Electrode/Electrolyte Interphases to Enable Wide Temperature Applications of Lithium-Ion Batteries. ACS Applied Materials & Interfaces, 2019, 11, 21496-21505.	4.0	44
117	A multi-functional interface derived from thiol-modified mesoporous carbon in lithium–sulfur batteries. Journal of Materials Chemistry A, 2019, 7, 13372-13381.	5.2	17
118	High-energy lithium metal pouch cells with limited anode swelling and long stable cycles. Nature Energy, 2019, 4, 551-559.	19.8	492
119	Injection of oxygen vacancies in the bulk lattice of layered cathodes. Nature Nanotechnology, 2019, 14, 602-608.	15.6	321
120	Self-smoothing anode for achieving high-energy lithium metal batteries under realistic conditions. Nature Nanotechnology, 2019, 14, 594-601.	15.6	451
121	High-Concentration Ether Electrolytes for Stable High-Voltage Lithium Metal Batteries. ACS Energy Letters, 2019, 4, 896-902.	8.8	302
122	Superionic conduction and interfacial properties of the low temperature phase Li7P2S8Br0.5l0.5. Energy Storage Materials, 2019, 19, 80-87.	9.5	39
123	High-quality mesoporous graphene particles as high-energy and fast-charging anodes for lithium-ion batteries. Nature Communications, 2019, 10, 1474.	5.8	140
124	Highly Stable Oxygen Electrodes Enabled by Catalyst Redistribution through an In Situ Electrochemical Method. Advanced Energy Materials, 2019, 9, 1803598.	10.2	6
125	Critical Parameters for Evaluating Coin Cells and Pouch Cells of Rechargeable Li-Metal Batteries. Joule, 2019, 3, 1094-1105.	11.7	358
126	Minimized Volume Expansion in Hierarchical Porous Silicon upon Lithiation. ACS Applied Materials & Interfaces, 2019, 11, 13257-13263.	4.0	51

#	Article	IF	CITATIONS
127	Good Practices for Rechargeable Lithium Metal Batteries. Journal of the Electrochemical Society, 2019, 166, A4141-A4149.	1.3	42
128	Creation and Ordering of Oxygen Vacancies at WO _{3â^îŕ} and Perovskite Interfaces. ACS Applied Materials & Interfaces, 2018, 10, 17480-17486.	4.0	29
129	Designing principle for Ni-rich cathode materials with high energy density for practical applications. Nano Energy, 2018, 49, 434-452.	8.2	400
130	Harnessing the concurrent reaction dynamics in active Si and Ge to achieve high performance lithium-ion batteries. Energy and Environmental Science, 2018, 11, 669-681.	15.6	329
131	Investigation of Ion–Solvent Interactions in Nonaqueous Electrolytes Using in Situ Liquid SIMS. Analytical Chemistry, 2018, 90, 3341-3348.	3.2	41
132	Enhanced Cyclability of Lithium–Oxygen Batteries with Electrodes Protected by Surface Films Induced via In Situ Electrochemical Process. Advanced Energy Materials, 2018, 8, 1702340.	10.2	38
133	Revealing the Reaction Mechanism of Na–O ₂ Batteries using Environmental Transmission Electron Microscopy. ACS Energy Letters, 2018, 3, 393-399.	8.8	30
134	Facet-Dependent Rock-Salt Reconstruction on the Surface of Layered Oxide Cathodes. Chemistry of Materials, 2018, 30, 692-699.	3.2	53
135	Simultaneous Stabilization of LiNi _{0.76} Mn _{0.14} Co _{0.10} O ₂ Cathode and Lithium Metal Anode by Lithium Bis(oxalato)borate as Additive. ChemSusChem, 2018, 11, 2211-2220.	3.6	89
136	Effect of calcination temperature on the electrochemical properties of nickel-rich LiNi0.76Mn0.14Co0.10O2 cathodes for lithium-ion batteries. Nano Energy, 2018, 49, 538-548.	8.2	213
137	High Voltage Operation of Niâ€Rich NMC Cathodes Enabled by Stable Electrode/Electrolyte Interphases. Advanced Energy Materials, 2018, 8, 1800297.	10.2	298
138	Structural Degradations in the Bulk of Cathode Particles for Li-ion Batteries. Microscopy and Microanalysis, 2018, 24, 1504-1505.	0.2	0
139	Morphology-Controlled Discharge Profile and Reversible Cu Extrusion and Dissolution in Biomimetic CuS. ACS Applied Materials & Interfaces, 2018, 10, 41458-41464.	4.0	8
140	Surface Gradient Ti-Doped MnO ₂ Nanowires for High-Rate and Long-Life Lithium Battery. ACS Applied Materials & Interfaces, 2018, 10, 44376-44384.	4.0	41
141	Solid–Liquid Interfacial Reaction Trigged Propagation of Phase Transition from Surface into Bulk Lattice of Ni-Rich Layered Cathode. Chemistry of Materials, 2018, 30, 7016-7026.	3.2	80
142	Frontiers of solid-state batteries. MRS Bulletin, 2018, 43, 740-745.	1.7	35
143	In Situ Transmission Electron Microsopy of Oxide Shell-Induced Pore Formation in (De)lithiated Silicon Nanowires. ACS Energy Letters, 2018, 3, 2829-2834.	8.8	25
144	Revealing Cycling Rate-Dependent Structure Evolution in Ni-Rich Layered Cathode Materials. ACS Energy Letters, 2018, 3, 2433-2440.	8.8	92

#	Article	IF	CITATIONS
145	Accessing crystal–crystal interaction forces with oriented nanocrystal atomic force microscopy probes. Nature Protocols, 2018, 13, 2005-2030.	5.5	12
146	High-Efficiency Lithium Metal Batteries with Fire-Retardant Electrolytes. Joule, 2018, 2, 1548-1558.	11.7	436
147	Synthesis and Electrochemical and Structural Investigations of Oxidatively Stable Li ₂ MoO ₃ and <i>x</i> Li ₂ MoO ₃ ·(1 –) Tj ETQq1 1 0.7843	14argBT /C)v ed ock 10 T
148	Coupling of electrochemically triggered thermal and mechanical effects to aggravate failure in a layered cathode. Nature Communications, 2018, 9, 2437.	5.8	200
149	Tailoring grain boundary structures and chemistry of Ni-rich layered cathodes for enhanced cycle stability of lithium-ion batteries. Nature Energy, 2018, 3, 600-605.	19.8	613
150	Stress-Tolerant Nanoporous Germanium Nanofibers for Long Cycle Life Lithium Storage with High Structural Stability. ACS Nano, 2018, 12, 8169-8176.	7.3	42
151	Mechanical mismatch-driven rippling in carbon-coated silicon sheets for stress-resilient battery anodes. Nature Communications, 2018, 9, 2924.	5.8	94
152	Size-dependent dynamic structures of supported gold nanoparticles in CO oxidation reaction condition. Proceedings of the National Academy of Sciences of the United States of America, 2018, 115, 7700-7705.	3.3	183
153	Atomic origins of water-vapour-promoted alloy oxidation. Nature Materials, 2018, 17, 514-518.	13.3	106
154	Observation of Solid-Liquid Interfacial Reactions Controlled Bulk Phase Transition of Ni-rich Layered Cathode. Microscopy and Microanalysis, 2018, 24, 1522-1523.	0.2	1
155	Revealing salt-expedited reduction mechanism for hollow silicon microsphere formation in bi-functional halide melts. Communications Chemistry, 2018, 1, .	2.0	31
156	Minimizing Polysulfide Shuttle Effect in Lithium-Ion Sulfur Batteries by Anode Surface Passivation. ACS Applied Materials & Interfaces, 2018, 10, 21965-21972.	4.0	18
157	Electrochemical and interfacial behavior of all solid state batteries using Li10SnP2S12 solid electrolyte. Journal of Power Sources, 2018, 396, 824-830.	4.0	54
158	B4C as a stable non-carbon-based oxygen electrode material for lithium-oxygen batteries. Nano Energy, 2017, 33, 195-204.	8.2	65
159	Intragranular cracking as a critical barrier for high-voltage usage of layer-structured cathode for lithium-ion batteries. Nature Communications, 2017, 8, 14101.	5.8	654
160	Oneâ€Pot Process for Hydrodeoxygenation of Lignin to Alkanes Using Ruâ€Based Bimetallic and Bifunctional Catalysts Supported on Zeolite Y. ChemSusChem, 2017, 10, 1846-1856.	3.6	127
161	Stabilization of Li Metal Anode in DMSOâ€Based Electrolytes via Optimization of Salt–Solvent Coordination for Li–O ₂ Batteries. Advanced Energy Materials, 2017, 7, 1602605.	10.2	99
162	Structural Transformations in High-Capacity Li ₂ Cu _{0.5} 0.5O ₂ Cathodes. Chemistry of Materials, 2017, 29, 2997-3005.	3.2	21

#	Article	IF	CITATIONS
163	Synthesis of an excellent electrocatalyst for oxygen reduction reaction with supercritical fluid: Graphene cellular monolith with ultrafine and highly dispersive multimetallic nanoparticles. Journal of Power Sources, 2017, 347, 69-78.	4.0	16
164	Formation of Reversible Solid Electrolyte Interface on Graphite Surface from Concentrated Electrolytes. Nano Letters, 2017, 17, 1602-1609.	4.5	91
165	Complete Decomposition of Li ₂ CO ₃ in Li–O ₂ Batteries Using Ir/B ₄ C as Noncarbon-Based Oxygen Electrode. Nano Letters, 2017, 17, 1417-1424.	4.5	104
166	Insights on the Mechanism of Na-Ion Storage in Soft Carbon Anode. Chemistry of Materials, 2017, 29, 2314-2320.	3.2	177
167	Tuning the Solid Electrolyte Interphase for Selective Li―and Naâ€ŀon Storage in Hard Carbon. Advanced Materials, 2017, 29, 1606860.	11.1	157
168	Atomic Layer Deposition of the Solid Electrolyte Garnet Li ₇ La ₃ Zr ₂ O ₁₂ . Chemistry of Materials, 2017, 29, 3785-3792.	3.2	149
169	Radiation Tolerant Interfaces: Influence of Local Stoichiometry at the Misfit Dislocation on Radiation Damage Resistance of Metal/Oxide Interfaces. Advanced Materials Interfaces, 2017, 4, 1700037.	1.9	10
170	Atomic Resolution Structural and Chemical Imaging Revealing the Sequential Migration of Ni, Co, and Mn upon the Battery Cycling of Layered Cathode. Nano Letters, 2017, 17, 3946-3951.	4.5	143
171	Design of porous Si/C–graphite electrodes with long cycle stability and controlled swelling. Energy and Environmental Science, 2017, 10, 1427-1434.	15.6	140
172	Direction-specific van der Waals attraction between rutile TiO ₂ nanocrystals. Science, 2017, 356, 434-437.	6.0	103
173	Rational Design of Hyperbranched Nanowire Systems for Tunable Superomniphobic Surfaces Enabled by Atomic Layer Deposition. ACS Nano, 2017, 11, 478-489.	7.3	54
174	Thermal Induced Strain Relaxation of 1D Iron Oxide for Solid Electrolyte Interphase Control and Lithium Storage Improvement. Advanced Energy Materials, 2017, 7, 1601582.	10.2	73
175	Wide-Temperature Electrolytes for Lithium-Ion Batteries. ACS Applied Materials & Interfaces, 2017, 9, 18826-18835.	4.0	150
176	Damage evolution of ion irradiated defected-fluorite La2Zr2O7 epitaxial thin films. Acta Materialia, 2017, 130, 111-120.	3.8	20
177	High-Performance Rh ₂ P Electrocatalyst for Efficient Water Splitting. Journal of the American Chemical Society, 2017, 139, 5494-5502.	6.6	343
178	Revealing the reaction mechanisms of Li–O2 batteries using environmental transmission electron microscopy. Nature Nanotechnology, 2017, 12, 535-539.	15.6	160
179	Li―and Mnâ€Rich Cathode Materials: Challenges to Commercialization. Advanced Energy Materials, 2017, 7, 1601284.	10.2	383
180	Temperature Dependence of the Oxygen Reduction Mechanism in Nonaqueous Li–O ₂ Batteries. ACS Energy Letters, 2017, 2, 2525-2530.	8.8	30

#	Article	IF	CITATIONS
181	Revealing the Dynamics of Platinum Nanoparticle Catalysts on Carbon in Oxygen and Water Using Environmental TEM. ACS Catalysis, 2017, 7, 7658-7664.	5.5	38
182	Formation of an Anti-Core–Shell Structure in Layered Oxide Cathodes for Li-Ion Batteries. ACS Energy Letters, 2017, 2, 2598-2606.	8.8	42
183	Rock-Salt Growth-Induced (003) Cracking in a Layered Positive Electrode for Li-Ion Batteries. ACS Energy Letters, 2017, 2, 2607-2615.	8.8	116
184	Single Atomic Iron Catalysts for Oxygen Reduction in Acidic Media: Particle Size Control and Thermal Activation. Journal of the American Chemical Society, 2017, 139, 14143-14149.	6.6	1,215
185	Suppressed oxygen extraction and degradation of LiNi x Mn y Co z O2 cathodes at high charge cut-off voltages. Nano Research, 2017, 10, 4221-4231.	5.8	77
186	Yolk-shell structured Sb@C anodes for high energy Na-ion batteries. Nano Energy, 2017, 40, 504-511.	8.2	123
187	Excess Li-Ion Storage on Reconstructed Surfaces of Nanocrystals To Boost Battery Performance. Nano Letters, 2017, 17, 6018-6026.	4.5	53
188	S/TEM Study of Fading Mechanism of Lithium Transition Metal Oxide Cathode for Lithium Ion Battery. Microscopy and Microanalysis, 2017, 23, 2016-2017.	0.2	1
189	Tuning the Outward to Inward Swelling in Lithiated Silicon Nanotubes via Surface Oxide Coating. Microscopy and Microanalysis, 2017, 23, 2018-2019.	0.2	0
190	Li ⁺ -Desolvation Dictating Lithium-Ion Battery's Low-Temperature Performances. ACS Applied Materials & Interfaces, 2017, 9, 42761-42768.	4.0	200
191	Tuning Li-Ion Diffusion in α-LiMn _{1–<i>x</i>} Fe _{<i>x</i>} PO ₄ Nanocrystals by Antisite Defects and Embedded β-Phase for Advanced Li-Ion Batteries. Nano Letters, 2017, 17, 4934-4940.	4.5	38
192	Nitrogen–doped graphitized carbon shell encapsulated NiFe nanoparticles: A highly durable oxygen evolution catalyst. Nano Energy, 2017, 39, 245-252.	8.2	143
193	Slip-activated surface creep with room-temperature super-elongation in metallicÂnanocrystals. Nature Materials, 2017, 16, 439-445.	13.3	82
194	In-Situ S/TEM and In-Situ SIMS Multi-Modality Probing of Chemical and Structural Evolution of Rechargeable Battery. Microscopy and Microanalysis, 2016, 22, 20-21.	0.2	0
195	Generation and the role of dislocations in single-crystalline phase-change In ₂ Se ₃ nanowires under electrical pulses. Nanotechnology, 2016, 27, 335704.	1.3	4
196	Enhanced Cycling Stability of Rechargeable Li–O ₂ Batteries Using High oncentration Electrolytes. Advanced Functional Materials, 2016, 26, 605-613.	7.8	104
197	Highly Stable Operation of Lithium Metal Batteries Enabled by the Formation of a Transient High oncentration Electrolyte Layer. Advanced Energy Materials, 2016, 6, 1502151.	10.2	236
198	Electrochemically Formed Ultrafine Metal Oxide Nanocatalysts for High-Performance Lithium–Oxygen Batteries. Nano Letters, 2016, 16, 4932-4939.	4.5	62

#	Article	IF	CITATIONS
199	Ni and Co Segregations on Selective Surface Facets and Rational Design of Layered Lithium Transitionâ€Metal Oxide Cathodes. Advanced Energy Materials, 2016, 6, 1502455.	10.2	100
200	Atomistic Conversion Reaction Mechanism of WO ₃ in Secondary Ion Batteries of Li, Na, and Ca. Angewandte Chemie - International Edition, 2016, 55, 6244-6247.	7.2	86
201	Characterization of electrical properties in axial Si-Ge nanowire heterojunctions using off-axis electron holography and atom-probe tomography. Journal of Applied Physics, 2016, 120, .	1.1	10
202	Transmission electron microscopy of specimens and processes in liquids. MRS Bulletin, 2016, 41, 791-803.	1.7	12
203	Multidimensional Analysis of Nanoscale Phase Separation in Complex Materials Systems. Microscopy and Microanalysis, 2016, 22, 282-283.	0.2	0
204	Size Dependent Pore Formation in Germanium Nanowires Undergoing Reversible Delithiation Observed by In Situ TEM. Journal of Physical Chemistry C, 2016, 120, 28825-28831.	1.5	9
205	Highly Reversible Zinc-Ion Intercalation into Chevrel Phase Mo ₆ S ₈ Nanocubes and Applications for Advanced Zinc-Ion Batteries. ACS Applied Materials & Interfaces, 2016, 8, 13673-13677.	4.0	256
206	Multimodal and <i>In-Situ</i> Chemical Imaging of Critical Surfaces and Interfaces in Li Batteries. Microscopy Today, 2016, 24, 32-39.	0.2	6
207	Electronegative guests in CoSb ₃ . Energy and Environmental Science, 2016, 9, 2090-2098.	15.6	93
208	Three-dimensional PtNi hollow nanochains as an enhanced electrocatalyst for the oxygen reduction reaction. Journal of Materials Chemistry A, 2016, 4, 8755-8761.	5.2	63
209	Competing Pathways for Nucleation of the Double Perovskite Structure in the Epitaxial Synthesis of La ₂ MnNiO ₆ . Chemistry of Materials, 2016, 28, 3814-3822.	3.2	29
210	Double Epitaxy as a Paradigm for Templated Growth of Highly Ordered Three-Dimensional Mesophase Crystals. ACS Nano, 2016, 10, 8670-8675.	7.3	2
211	Exploring Lithium-Cobalt-Nickel Oxide Spinel Electrodes for ≥3.5 V Li-Ion Cells. ACS Applied Materials & Interfaces, 2016, 8, 27720-27729.	4.0	25
212	The importance of solid electrolyte interphase formation for long cycle stability full-cell Na-ion batteries. Nano Energy, 2016, 27, 664-672.	8.2	41
213	Hard carbon coated nano-Si/graphite composite as a high performance anode for Li-ion batteries. Journal of Power Sources, 2016, 329, 323-329.	4.0	73
214	Electron Transfer Governed Crystal Transformation of Tungsten Trioxide upon Li Ions Intercalation. ACS Applied Materials & Interfaces, 2016, 8, 24567-24572.	4.0	26
215	Tuning the Outward to Inward Swelling in Lithiated Silicon Nanotubes via Surface Oxide Coating. Nano Letters, 2016, 16, 5815-5822.	4.5	45
216	In Situ and Ex Situ TEM Study of Lithiation Behaviours of Porous Silicon Nanostructures. Scientific Reports, 2016, 6, 31334.	1.6	43

#	Article	IF	CITATIONS
217	Tuning of Thermal Stability in Layered Li(Ni _{<i>x</i>} Mn _{<i>y</i>} Co _{<i>z</i>})O ₂ . Journal of the American Chemical Society, 2016, 138, 13326-13334.	6.6	178
218	In situ observation of shear-driven amorphization in silicon crystals. Nature Nanotechnology, 2016, 11, 866-871.	15.6	74
219	Making ultrafine and highly-dispersive multimetallic nanoparticles in three-dimensional graphene with supercritical fluid as excellent electrocatalyst for oxygen reduction reaction. Journal of Materials Chemistry A, 2016, 4, 18628-18638.	5.2	29
220	SnO ₂ Quantum Dots@Graphene Oxide as a Highâ€Rate and Longâ€Life Anode Material for Lithiumâ€Ion Batteries. Small, 2016, 12, 588-594.	5.2	338
221	Atomistic Conversion Reaction Mechanism of WO ₃ in Secondary Ion Batteries of Li, Na, and Ca. Angewandte Chemie, 2016, 128, 6352-6355.	1.6	21
222	Direct Mapping of Charge Distribution during Lithiation of Ge Nanowires Using Off-Axis Electron Holography. Nano Letters, 2016, 16, 3748-3753.	4.5	34
223	A facile cathode design combining Ni-rich layered oxides with Li-rich layered oxides for lithium-ion batteries. Journal of Power Sources, 2016, 325, 620-629.	4.0	46
224	Ultrathin Li ₄ Ti ₅ O ₁₂ Nanosheets as Anode Materials for Lithium and Sodium Storage. ACS Applied Materials & amp; Interfaces, 2016, 8, 16718-16726.	4.0	87
225	In situ atomic scale visualization of surface kinetics driven dynamics of oxide growth on a Ni–Cr surface. Chemical Communications, 2016, 52, 3300-3303.	2.2	38
226	A Spinel-Integrated P2-Type Layered Composite: High-Rate Cathode for Sodium-Ion Batteries. Journal of the Electrochemical Society, 2016, 163, A584-A591.	1.3	57
227	In-situ transmission electron microscopy study of surface oxidation for Ni–10Cr and Ni–20Cr alloys. Scripta Materialia, 2016, 114, 129-132.	2.6	43
228	Effects of Propylene Carbonate Content in CsPF ₆ -Containing Electrolytes on the Enhanced Performances of Graphite Electrode for Lithium-Ion Batteries. ACS Applied Materials & Interfaces, 2016, 8, 5715-5722.	4.0	43
229	Germanium as a Sodium Ion Battery Material: <i>In Situ</i> TEM Reveals Fast Sodiation Kinetics with High Capacity. Chemistry of Materials, 2016, 28, 1236-1242.	3.2	134
230	A stable nanoporous silicon anode prepared by modified magnesiothermic reactions. Nano Energy, 2016, 20, 68-75.	8.2	65
231	Atomic to Nanoscale Investigation of Functionalities of an Al ₂ O ₃ Coating Layer on a Cathode for Enhanced Battery Performance. Chemistry of Materials, 2016, 28, 857-863.	3.2	125
232	Size-Controlled Intercalation-to-Conversion Transition in Lithiation of Transition-Metal Chalcogenides—NbSe ₃ . ACS Nano, 2016, 10, 1249-1255.	7.3	29
233	Graphene Oxide Wrapped Amorphous Copper Vanadium Oxide with Enhanced Capacitive Behavior for Highâ€Rate and Longâ€Life Lithiumâ€Ion Battery Anodes. Advanced Science, 2015, 2, 1500154.	5.6	114
234	Structural and Chemical Evolution of Li and Mn Rich Layered Oxide Cathode and Correlation with Capacity and Voltage Fading. Microscopy and Microanalysis, 2015, 21, 141-142.	0.2	1

#	Article	IF	CITATIONS
235	Direct in Situ TEM Observation of Modification of Oxidation by the Injected Vacancies for Ni–4Al Alloy Using a Microfabricated Nanopost. ACS Applied Materials & Interfaces, 2015, 7, 17272-17277.	4.0	35
236	Interface Promoted Reversible Mg Insertion in Nanostructured Tin–Antimony Alloys. Advanced Materials, 2015, 27, 6598-6605.	11.1	88
237	Inâ€Situâ€Grown ZnCo ₂ O ₄ on Singleâ€Walled Carbon Nanotubes as Air Electrode Materials for Rechargeable Lithium–Oxygen Batteries. ChemSusChem, 2015, 8, 3697-3703.	3.6	34
238	Probing the failure mechanism of nanoscale LiFePO4 for Li-ion batteries. Applied Physics Letters, 2015, 106, 203902.	1.5	15
239	General synthesis of complex nanotubes by gradient electrospinning and controlled pyrolysis. Nature Communications, 2015, 6, 7402.	5.8	370
240	Inward lithium-ion breathing of hierarchically porous silicon anodes. Nature Communications, 2015, 6, 8844.	5.8	217
241	In Situ TEM Observations of Sn-Containing Silicon Nanowires Undergoing Reversible Pore Formation Due to Fast Lithiation/Delithiation Kinetics. Journal of Physical Chemistry C, 2015, 119, 21889-21895.	1.5	38
242	Observation of Electron-Beam-Induced Phase Evolution Mimicking the Effect of the Charge–Discharge Cycle in Li-Rich Layered Cathode Materials Used for Li Ion Batteries. Chemistry of Materials, 2015, 27, 1375-1380.	3.2	73
243	Strong kinetics-stress coupling in lithiation of Si and Ge anodes. Extreme Mechanics Letters, 2015, 2, 1-6.	2.0	66
244	Regulated Breathing Effect of Silicon Negative Electrode for Dramatically Enhanced Performance of Liâ€ion Battery. Advanced Functional Materials, 2015, 25, 1426-1433.	7.8	149
245	Tailoring Pore Size of Nitrogenâ€Đoped Hollow Carbon Nanospheres for Confining Sulfur in Lithium–Sulfur Batteries. Advanced Energy Materials, 2015, 5, 1401752.	10.2	273
246	Structural and Chemical Evolution of Li- and Mn-Rich Layered Cathode Material. Chemistry of Materials, 2015, 27, 1381-1390.	3.2	311
247	In situ transmission electron microscopy observations of lithiation of spherical silicon nanopowder produced by induced plasma atomization. Journal of Power Sources, 2015, 279, 522-527.	4.0	14
248	Nanocomposite polymer electrolyte for rechargeable magnesium batteries. Nano Energy, 2015, 12, 750-759.	8.2	121
249	Realizing the Full Potential of Insertion Anodes for Mg-Ion Batteries Through the Nanostructuring of Sn. Nano Letters, 2015, 15, 1177-1182.	4.5	87
250	Probing the Degradation Mechanism of Li ₂ MnO ₃ Cathode for Li-Ion Batteries. Chemistry of Materials, 2015, 27, 975-982.	3.2	130
251	Kinetics Tuning of Li-Ion Diffusion in Layered Li(Ni _{<i>x</i>} Mn _{<i>y</i>} Co _{<i>z</i>})O ₂ . Journal of the American Chemical Society, 2015, 137, 8364-8367.	6.6	292
252	Atomic-Resolution Visualization of Distinctive Chemical Mixing Behavior of Ni, Co, and Mn with Li in Layered Lithium Transition-Metal Oxide Cathode Materials. Chemistry of Materials, 2015, 27, 5393-5401.	3.2	108

#	Article	IF	CITATIONS
253	High performance Li-ion sulfur batteries enabled by intercalation chemistry. Chemical Communications, 2015, 51, 13454-13457.	2.2	55
254	Effects of structural defects on the electrochemical activation of Li2MnO3. Nano Energy, 2015, 16, 143-151.	8.2	73
255	Iron Atom Exchange between Hematite and Aqueous Fe(II). Environmental Science & Technology, 2015, 49, 8479-8486.	4.6	99
256	Surface-Coating Regulated Lithiation Kinetics and Degradation in Silicon Nanowires for Lithium Ion Battery. ACS Nano, 2015, 9, 5559-5566.	7.3	118
257	Crystallographic dependence of photocatalytic activity of WO ₃ thin films prepared by molecular beam epitaxy. Physical Chemistry Chemical Physics, 2015, 17, 15119-15123.	1.3	32
258	Following the Transient Reactions in Lithium–Sulfur Batteries Using an In Situ Nuclear Magnetic Resonance Technique. Nano Letters, 2015, 15, 3309-3316.	4.5	107
259	Observation of materials processes in liquids by electron microscopy. MRS Bulletin, 2015, 40, 46-52.	1.7	40
260	Surface Coating Constraint Induced Self-Discharging of Silicon Nanoparticles as Anodes for Lithium Ion Batteries. Nano Letters, 2015, 15, 7016-7022.	4.5	113
261	Nanoscale silicon as anode for Li-ion batteries: The fundamentals, promises, and challenges. Nano Energy, 2015, 17, 366-383.	8.2	228
262	Phosphorus Enrichment as a New Composition in the Solid Electrolyte Interphase of High-Voltage Cathodes and Its Effects on Battery Cycling. Chemistry of Materials, 2015, 27, 7447-7451.	3.2	37
263	In Situ Mass Spectrometric Determination of Molecular Structural Evolution at the Solid Electrolyte Interphase in Lithium-Ion Batteries. Nano Letters, 2015, 15, 6170-6176.	4.5	73
264	The Role of Cesium Cation in Controlling Interphasial Chemistry on Graphite Anode in Propylene Carbonate-Rich Electrolytes. ACS Applied Materials & Interfaces, 2015, 7, 20687-20695.	4.0	41
265	Evolution of Lattice Structure and Chemical Composition of the Surface Reconstruction Layer in Li _{1.2} Ni _{0.2} Mn _{0.6} O ₂ Cathode Material for Lithium Ion Batteries. Nano Letters, 2015, 15, 514-522.	4.5	261
266	In situ transmission electron microscopy and spectroscopy studies of rechargeable batteries under dynamic operating conditions: A retrospective and perspective view. Journal of Materials Research, 2015, 30, 326-339.	1.2	108
267	ROS/p38/p53/Puma signaling pathway is involved in emodin-induced apoptosis of human colorectal cancer cells. International Journal of Clinical and Experimental Medicine, 2015, 8, 15413-22.	1.3	25
268	<i>In Situ</i> Transmission Electron Microscopy Probing of Native Oxide and Artificial Layers on Silicon Nanoparticles for Lithium Ion Batteries. ACS Nano, 2014, 8, 11816-11823.	7.3	99
269	Interface modifications by anion receptors for high energy lithium ion batteries. Journal of Power Sources, 2014, 250, 313-318.	4.0	74
270	A facile approach using MgCl2 to formulate high performance Mg2+ electrolytes for rechargeable Mg batteries. Journal of Materials Chemistry A, 2014, 2, 3430.	5.2	197

#	Article	IF	CITATIONS
271	Nanorod Niobium Oxide as Powerful Catalysts for an All Vanadium Redox Flow Battery. Nano Letters, 2014, 14, 158-165.	4.5	279
272	Direct Evidence of Lithium-Induced Atomic Ordering in Amorphous TiO ₂ Nanotubes. Chemistry of Materials, 2014, 26, 1660-1669.	3.2	75
273	High-performance anode based on porous Co3O4 nanodiscs. Journal of Power Sources, 2014, 255, 125-129.	4.0	67
274	Lithium Ion Battery Peformance of Silicon Nanowires with Carbon Skin. ACS Nano, 2014, 8, 915-922.	7.3	185
275	TEM study of fivefold twined gold nanocrystal formation mechanism. Materials Letters, 2014, 116, 299-303.	1.3	19
276	Controlling SEI Formation on SnSbâ€Porous Carbon Nanofibers for Improved Na Ion Storage. Advanced Materials, 2014, 26, 2901-2908.	11.1	441
277	Functioning Mechanism of AlF ₃ Coating on the Li- and Mn-Rich Cathode Materials. Chemistry of Materials, 2014, 26, 6320-6327.	3.2	333
278	Chemical bonding in amorphous Si-coated carbon nanotubes as anodes for Li ion batteries: a XANES study. RSC Advances, 2014, 4, 20226-20229.	1.7	17
279	Fe(II)-Catalyzed Recrystallization of Goethite Revisited. Environmental Science & Technology, 2014, 48, 11302-11311.	4.6	160
280	Formation of Interfacial Layer and Long-Term Cyclability of Li–O ₂ Batteries. ACS Applied Materials & Interfaces, 2014, 6, 14141-14151.	4.0	44
281	Bending-Induced Symmetry Breaking of Lithiation in Germanium Nanowires. Nano Letters, 2014, 14, 4622-4627.	4.5	92
282	Enhancing the lithiation rate of silicon nanowires by the inclusion of tin. RSC Advances, 2014, 4, 42022-42028.	1.7	20
283	Strain Accommodation by Facile WO ₆ Octahedral Distortion and Tilting during WO ₃ Heteroepitaxy on SrTiO ₃ (001). ACS Applied Materials & Interfaces, 2014, 6, 14253-14258.	4.0	29
284	Facile Synthesis of <i>Chevrel</i> Phase Nanocubes and Their Applications for Multivalent Energy Storage. Chemistry of Materials, 2014, 26, 4904-4907.	3.2	73
285	Lewis Acid–Base Interactions between Polysulfides and Metal Organic Framework in Lithium Sulfur Batteries. Nano Letters, 2014, 14, 2345-2352.	4.5	623
286	Mesoporous silicon sponge as an anti-pulverization structure for high-performance lithium-ion battery anodes. Nature Communications, 2014, 5, 4105.	5.8	1,160
287	Molecular structure and stability of dissolved lithium polysulfide species. Physical Chemistry Chemical Physics, 2014, 16, 10923-10932.	1.3	210
288	Mitigating Voltage Fade in Cathode Materials by Improving the Atomic Level Uniformity of Elemental Distribution. Nano Letters, 2014, 14, 2628-2635.	4.5	273

#	Article	IF	CITATIONS
289	Dual phase Li4Ti5O12–TiO2 nanowire arrays as integrated anodes for high-rate lithium-ion batteries. Nano Energy, 2014, 9, 383-391.	8.2	114
290	Probing the Degradation Mechanisms in Electrolyte Solutions for Li-Ion Batteries by in Situ Transmission Electron Microscopy. Nano Letters, 2014, 14, 1293-1299.	4.5	137
291	Defect structure of epitaxial CrxV1â°x thin films on MgO(001). Thin Solid Films, 2014, 550, 1-9.	0.8	8
292	Revealing the Atomic Restructuring of Pt–Co Nanoparticles. Nano Letters, 2014, 14, 3203-3207.	4.5	162
293	Highly Reversible Mg Insertion in Nanostructured Bi for Mg Ion Batteries. Nano Letters, 2014, 14, 255-260.	4.5	257
294	Mesoscale Origin of the Enhanced Cycling-Stability of the Si-Conductive Polymer Anode for Li-ion Batteries. Scientific Reports, 2014, 4, 3684.	1.6	43
295	In-Situ TEM visualization of vacancy injection and chemical partition during oxidation of Ni-Cr nanoparticles. Scientific Reports, 2014, 4, 3683.	1.6	53
296	Materials Science and Materials Chemistry for Large Scale Electrochemical Energy Storage: From Transportation to Electrical Grid. Advanced Functional Materials, 2013, 23, 929-946.	7.8	590
297	First principles prediction of nitrogen-doped carbon nanotubes as a high-performance cathode for Li–S batteries. RSC Advances, 2013, 3, 16775.	1.7	44
298	Probing the Failure Mechanism of SnO ₂ Nanowires for Sodium-Ion Batteries. Nano Letters, 2013, 13, 5203-5211.	4.5	270
299	Demonstration of an Electrochemical Liquid Cell for Operando Transmission Electron Microscopy Observation of the Lithiation/Delithiation Behavior of Si Nanowire Battery Anodes. Nano Letters, 2013, 13, 6106-6112.	4.5	265
300	Bifunctional nanoparticles for SERS monitoring and magnetic intervention of assembly and enzyme cutting of DNAs. Journal of Materials Chemistry B, 2013, 1, 4320.	2.9	27
301	Corrosion/Fragmentation of Layered Composite Cathode and Related Capacity/Voltage Fading during Cycling Process. Nano Letters, 2013, 13, 3824-3830.	4.5	353
302	Electron-Rich Driven Electrochemical Solid-State Amorphization in Li–Si Alloys. Nano Letters, 2013, 13, 4511-4516.	4.5	51
303	XEDS STEM tomography for 3D chemical characterization of nanoscale particles. Ultramicroscopy, 2013, 131, 24-32.	0.8	78
304	Catalytic templating approaches for three-dimensional hollow carbon/graphene oxide nano-architectures. Nanoscale, 2013, 5, 6291.	2.8	31
305	Very Stable Electron Field Emission from Strontium Titanate Coated Carbon Nanotube Matrices with Low Emission Thresholds. ACS Nano, 2013, 7, 117-125.	7.3	60
306	Structure and radiation damage behavior of epitaxial Cr Mo1â^ alloy thin films on MgO. Journal of Nuclear Materials, 2013, 437, 55-61.	1.3	6

#	Article	IF	CITATIONS
307	Electrochemical Kinetics and Performance of Layered Composite Cathode Material Li[Li _{0.2} Ni _{0.2} Mn _{0.6}]O ₂ . Journal of the Electrochemical Society, 2013, 160, A2212-A2219.	1.3	104
308	Formation of the Spinel Phase in the Layered Composite Cathode Used in Li-Ion Batteries. ACS Nano, 2013, 7, 760-767.	7.3	772
309	Enhanced Intercalation Dynamics and Stability of Engineered Micro/Nano tructured Electrode Materials: Vanadium Oxide Mesocrystals. Small, 2013, 9, 3880-3886.	5.2	50
310	In Situ TEM of Two-Phase Lithiation of Amorphous Silicon Nanospheres. Nano Letters, 2013, 13, 758-764.	4.5	680
311	Bismuth Nanoparticle Decorating Graphite Felt as a High-Performance Electrode for an All-Vanadium Redox Flow Battery. Nano Letters, 2013, 13, 1330-1335.	4.5	392
312	Nanoscale Phase Separation, Cation Ordering, and Surface Chemistry in Pristine Li _{1.2} Ni _{0.2} Mn _{0.6} O ₂ for Li-Ion Batteries. Chemistry of Materials, 2013, 25, 2319-2326.	3.2	173
313	Nanostructured materials for rechargeable batteries: synthesis, fundamental understanding and limitations. Current Opinion in Chemical Engineering, 2013, 2, 151-159.	3.8	7
314	Tomography and High-Resolution Electron Microscopy Study of Surfaces and Porosity in a Plate-like γ-Al ₂ O ₃ . Journal of Physical Chemistry C, 2013, 117, 179-186.	1.5	81
315	Electronic Origin for the Phase Transition from Amorphous Li _{<i>x</i>} Si to Crystalline Li ₁₅ Si ₄ . ACS Nano, 2013, 7, 6303-6309.	7.3	135
316	Interfaces: Ultralow Contact Resistance at an Epitaxial Metal/Oxide Heterojunction Through Interstitial Site Doping (Adv. Mater. 29/2013). Advanced Materials, 2013, 25, 3926-3926.	11.1	0
317	Ultralow Contact Resistance at an Epitaxial Metal/Oxide Heterojunction Through Interstitial Site Doping. Advanced Materials, 2013, 25, 4001-4005.	11.1	24
318	Controlled Nucleation and Growth Process of Li ₂ S ₂ /Li ₂ S in Lithium-Sulfur Batteries. Journal of the Electrochemical Society, 2013, 160, A1992-A1996.	1.3	89
319	How to Obtain Reproducible Results for Lithium Sulfur Batteries?. Journal of the Electrochemical Society, 2013, 160, A2288-A2292.	1.3	149
320	Revisit Carbon/Sulfur Composite for Li-S Batteries. Journal of the Electrochemical Society, 2013, 160, A1624-A1628.	1.3	98
321	In Situ TEM Investigation of Congruent Phase Transition and Structural Evolution of Nanostructured Silicon/Carbon Anode for Lithium Ion Batteries. Nano Letters, 2012, 12, 1624-1632.	4.5	256
322	<i>In Situ</i> TEM Study of Lithiation Behavior of Silicon Nanoparticles Attached to and Embedded in a Carbon Matrix. ACS Nano, 2012, 6, 8439-8447.	7.3	321
323	Highly Dispersed and Active ReO _{<i>x</i>} on Alumina-Modified SBA-15 Silica for 2-Butanol Dehydration. ACS Catalysis, 2012, 2, 1020-1026.	5.5	22
324	The effect of metallic coatings and crystallinity on the volume expansion of silicon during electrochemical lithiation/delithiation. Nano Energy, 2012, 1, 401-410.	8.2	156

#	Article	IF	CITATIONS
325	Studying the Kinetics of Crystalline Silicon Nanoparticle Lithiation with In Situ Transmission Electron Microscopy. Advanced Materials, 2012, 24, 6034-6041.	11.1	529
326	Factors affecting the battery performance of anthraquinone-based organic cathode materials. Journal of Materials Chemistry, 2012, 22, 4032.	6.7	126
327	Conflicting Roles of Nickel in Controlling Cathode Performance in Lithium Ion Batteries. Nano Letters, 2012, 12, 5186-5191.	4.5	231
328	Carbon dioxide-assisted fabrication of highly uniform submicron-sized colloidal carbon spheres via hydrothermal carbonization using soft drink. Colloid and Polymer Science, 2012, 290, 1567-1573.	1.0	17
329	Hollow core–shell structured porous Si–C nanocomposites for Li-ion battery anodes. Journal of Materials Chemistry, 2012, 22, 11014.	6.7	280
330	A Yolk-Shell Design for Stabilized and Scalable Li-Ion Battery Alloy Anodes. Nano Letters, 2012, 12, 3315-3321.	4.5	1,587
331	Template free synthesis of LiV ₃ O ₈ nanorods as a cathode material for high-rate secondary lithium batteries. Journal of Materials Chemistry, 2011, 21, 1153-1161.	6.7	105
332	A New Geometric Method Based on Two-Dimensional Transmission Electron Microscopy for Analysis of Interior versus Exterior Pd Loading on Hollow Carbon Nanofibers. Journal of Physical Chemistry Letters, 2011, 2, 1082-1087.	2.1	3
333	Monodisperse Au ₁₁ Clusters Prepared by Soft Landing of Mass Selected Ions. Analytical Chemistry, 2011, 83, 8069-8072.	3.2	49
334	Competitive Reduction of Pertechnetate (⁹⁹ TcO ₄ ^{â^'}) by Dissimilatory Metal Reducing Bacteria and Biogenic Fe(II). Environmental Science & Technology, 2011, 45, 951-957.	4.6	48
335	Nanosheet-structured LiV3O8 with high capacity and excellent stability for high energy lithium batteries. Journal of Materials Chemistry, 2011, 21, 10077.	6.7	112
336	The role of H2O in the carbonation of forsterite in supercritical CO2. International Journal of Greenhouse Gas Control, 2011, 5, 1081-1092.	2.3	103
337	Stabilization of Electrocatalytic Metal Nanoparticles at Metalâ^'Metal Oxideâ^'Graphene Triple Junction Points. Journal of the American Chemical Society, 2011, 133, 2541-2547.	6.6	391
338	In Situ Transmission Electron Microscopy Observation of Microstructure and Phase Evolution in a SnO ₂ Nanowire during Lithium Intercalation. Nano Letters, 2011, 11, 1874-1880.	4.5	266
339	The Effect of Stocking Densities on Reproductive Performance in Laboratory Zebrafish (<i>Danio) Tj ETQq1 1 0.78</i>	34314 rgB 0.5	T /Qverlock
340	The mineralogic transformation of ferrihydrite induced by heterogeneous reaction with bioreduced anthraquinone disulfonate (AQDS) and the role of phosphate. Geochimica Et Cosmochimica Acta, 2011, 75, 6330-6349.	1.6	33
341	Direct Conversion of Bio-ethanol to Isobutene on Nanosized Zn _{<i>x</i>} Zr _{<i>y</i>} O _{<i>z</i>} Mixed Oxides with Balanced Acid–Base Sites. Journal of the American Chemical Society, 2011, 133, 11096-11099.	6.6	225
342	Effect of reductive treatments on Pt behavior and NOx storage in lean NOx trap catalysts. Catalysis Today, 2011, 175, 78-82.	2.2	4

#	Article	IF	CITATIONS
343	Preparation and electrochemical investigation of Li2CoPO4F cathode material for lithium-ion batteries. Journal of Power Sources, 2011, 196, 2241-2245.	4.0	58
344	Structure of Cr film epitaxially grown on MgO(001). Acta Materialia, 2011, 59, 4274-4282.	3.8	22
345	Microstructure of the Native Oxide Layer on Ni and Cr-Doped Ni Nanoparticles. Journal of Nanoscience and Nanotechnology, 2011, 11, 8488-8497.	0.9	21
346	Nitrogen-doped mesoporous carbon for energy storage in vanadium redox flow batteries. Journal of Power Sources, 2010, 195, 4375-4379.	4.0	306
347	Ethanol synthesis from syngas over Rh-based/SiO2 catalysts: A combined experimental and theoretical modeling study. Journal of Catalysis, 2010, 271, 325-342.	3.1	174
348	Vapor-induced solid–liquid–solid process for silicon-based nanowire growth. Journal of Power Sources, 2010, 195, 1691-1697.	4.0	16
349	Noncovalently functionalized graphitic mesoporous carbon as a stable support of Pt nanoparticles for oxygen reduction. Journal of Power Sources, 2010, 195, 1805-1811.	4.0	78
350	Highly durable graphene nanoplatelets supported Pt nanocatalysts for oxygen reduction. Journal of Power Sources, 2010, 195, 4600-4605.	4.0	378
351	In situ transmission electron microscopy and spectroscopy studies of interfaces in Li ion batteries: Challenges and opportunities. Journal of Materials Research, 2010, 25, 1541-1547.	1.2	112
352	Coreâ~'Shell-Structured Magnetic Ternary Nanocubes. Journal of the American Chemical Society, 2010, 132, 17686-17689.	6.6	45
353	Synthesis, Characterization, and Application of Metal Organic Framework Nanostructures. Langmuir, 2010, 26, 18591-18594.	1.6	22
354	From Ultrafine Thiolate-Capped Copper Nanoclusters toward Copper Sulfide Nanodiscs: A Thermally Activated Evolution Route. Chemistry of Materials, 2010, 22, 261-271.	3.2	77
355	Facile and controllable electrochemical reduction of graphene oxide and its applications. Journal of Materials Chemistry, 2010, 20, 743-748.	6.7	787
356	The Durability Dependence of Pt/CNT Electrocatalysts on the Nanostructures of Carbon Nanotubes: Hollow- and Bamboo-CNTs. Journal of Nanoscience and Nanotechnology, 2009, 9, 5811-5815.	0.9	13
357	Damage profile and ion distribution of slow heavy ions in compounds. Journal of Applied Physics, 2009, 105, .	1.1	85
358	Fluorescent dye encapsulated ZnO particles with cell-specific toxicity for potential use in biomedical applications. Journal of Materials Science: Materials in Medicine, 2009, 20, 11-22.	1.7	121
359	Advancements Toward the Greener Processing of Engineered Nanomaterials—Effect of Core Size on the Dispersibility and Transport of Gold Nanocrystals in Nearâ€Critical Solvents. Small, 2009, 5, 961-969.	5.2	8
360	A novel low-temperature dendritic cyclotrimerization of 2,6-diacetyl pyridine leading to mesoporous carbon containing pyridine rings. Microporous and Mesoporous Materials, 2009, 123, 345-348.	2.2	10

#	Article	IF	CITATIONS
361	Enhanced activity and stability of Pt catalysts on functionalized graphene sheets for electrocatalytic oxygen reduction. Electrochemistry Communications, 2009, 11, 954-957.	2.3	615
362	Controlled deposition of covalently bonded tantalum oxide on carbon supports by solvent evaporation sol–gel process. Surface Science, 2009, 603, 2290-2293.	0.8	11
363	Self-Assembled TiO ₂ –Graphene Hybrid Nanostructures for Enhanced Li-Ion Insertion. ACS Nano, 2009, 3, 907-914.	7.3	1,596
364	Uranium in Framboidal Pyrite from a Naturally Bioreduced Alluvial Sediment. Environmental Science & Technology, 2009, 43, 8528-8534.	4.6	85
365	Effect of Chemical Lithium Insertion into Rutile TiO ₂ Nanorods. Journal of Physical Chemistry C, 2009, 113, 14567-14574.	1.5	59
366	Effect of the Ligand Shell Composition on the Dispersibility and Transport of Gold Nanocrystals in Near-Critical Solvents. Langmuir, 2009, 25, 4900-4906.	1.6	10
367	Stabilization of Metal Nanoparticles in Cubic Mesostructured Silica and Its Application in Regenerable Deep Desulfurization of Warm Syngas. Chemistry of Materials, 2009, 21, 5358-5364.	3.2	37
368	Glucose biosensor based on immobilization of glucose oxidase in platinum nanoparticles/graphene/chitosan nanocomposite film. Talanta, 2009, 80, 403-406.	2.9	416
369	Morphology and Electronic Structure of the Oxide Shell on the Surface of Iron Nanoparticles. Journal of the American Chemical Society, 2009, 131, 8824-8832.	6.6	218
370	Rapid synthesis and size control of CuInS2 semi-conductor nanoparticles using microwave irradiation. Journal of Nanoparticle Research, 2008, 10, 633-641.	0.8	82
371	The synthesis of Ag-doped mesoporous TiO2. Microporous and Mesoporous Materials, 2008, 111, 639-642.	2.2	29
372	Investigation of iron–chromium–niobium–titanium ferritic stainless steel for solid oxide fuel cell interconnect applications. Journal of Power Sources, 2008, 183, 660-667.	4.0	91
373	Low-Temperature Synthesis of Tunable Mesoporous Crystalline Transition Metal Oxides and Applications as Au Catalyst Supports. Journal of Physical Chemistry C, 2008, 112, 13499-13509.	1.5	81
374	Effect of nickel microstructure on methane steam-reforming activity of Ni–YSZ cermet anode catalyst. Journal of Catalysis, 2008, 258, 356-365.	3.1	67
375	Synthesis and Li-Ion Insertion Properties of Highly Crystalline Mesoporous Rutile TiO ₂ . Chemistry of Materials, 2008, 20, 3435-3442.	3.2	254
376	Tuning and Quantifying the Dispersibility of Gold Nanocrystals in Liquid and Supercritical Solvents. Journal of Physical Chemistry C, 2008, 112, 13947-13957.	1.5	13
377	Tilted domain growth of metalorganic chemical vapor (MOCVD)-grown ZnO(0001) on α-Al ₂ O ₃ (0001). Journal of Materials Research, 2008, 23, 13-17.	1.2	4
378	Proton dynamics in ZnO nanorods quantified by <i>in situ</i> solid-state H1 nuclear magnetic resonance spectroscopy. Applied Physics Letters, 2007, 91, .	1.5	14

#	Article	IF	CITATIONS
379	Hydrothermal Dehydration of Aqueous Fructose Solutions in a Closed System. Journal of Physical Chemistry C, 2007, 111, 15141-15145.	1.5	266
380	Synthesis and photoexcited charge carrier dynamics of β-FeOOH nanorods. Applied Physics Letters, 2007, 90, 103504.	1.5	13
381	Understanding Practical Catalysts Using a Surface Science Approach:  The Importance of Strong Interaction between BaO and Al ₂ O ₃ in NO <i>_x</i> Storage Materials. Journal of Physical Chemistry C, 2007, 111, 14942-14944.	1.5	32
382	Growth and structure of MBE grown TiO2 anatase films with rutile nano-crystallites. Surface Science, 2007, 601, 1582-1589.	0.8	25
383	Electron beam-induced thickening of the protective oxide layer around Fe nanoparticles. Ultramicroscopy, 2007, 108, 43-51.	0.8	53
384	Synthesis and characterization of phosphate-coated mesoporous titania and Cd-doping of same via ion-exchange. Inorganic Chemistry Communication, 2007, 10, 642-645.	1.8	12
385	The synthesis of cadmium doped mesoporous TiO2. Inorganic Chemistry Communication, 2007, 10, 639-641.	1.8	19
386	Templating mesoporous hierarchies in silica thin films using the thermal degradation of cellulose nitrate. Microporous and Mesoporous Materials, 2007, 99, 308-318.	2.2	9
387	Synthesis of SiC nanorods from bleached wood pulp. Materials Letters, 2007, 61, 2814-2817.	1.3	38
388	Preparation of Ultrafine Chalcopyrite Nanoparticles via the Photochemical Decomposition of Molecular Single-Source Precursors. Nano Letters, 2006, 6, 1218-1223.	4.5	164
389	Excited Carrier Dynamics of α-Cr2O3/α-Fe2O3 Coreâ^'Shell Nanostructures. Journal of Physical Chemistry B, 2006, 110, 16937-16940.	1.2	19
390	Synthesis of Organically Templated Nanoporous Tin(II/IV) Phosphate for Radionuclide and Metal Sequestration. Inorganic Chemistry, 2006, 45, 2382-2384.	1.9	25
391	Morphological Evolution of Ba(NO3)2Supported on α-Al2O3(0001): An In Situ TEM Study. Journal of Physical Chemistry B, 2006, 110, 11878-11883.	1.2	7
392	Synthesis and Characterization of Stable Iron–Iron Oxide Core–Shell Nanoclusters for Environmental Applications. Journal of Nanoscience and Nanotechnology, 2006, 6, 568-572.	0.9	35
393	Nitrocellulose templated hierarchical pore structure in mesoporous thin films. Inorganic Chemistry Communication, 2006, 9, 7-9.	1.8	11
394	Effects of Ba loading and calcination temperature on BaAl2O4 formation for BaO/Al2O3 NOx storage and reduction catalysts. Catalysis Today, 2006, 114, 86-93.	2.2	70
395	Microstructure of ZrO2–CeO2 hetero-multi-layer films grown on YSZ substrate. Acta Materialia, 2005, 53, 1921-1929.	3.8	29
396	Characterization and Properties of Metallic Iron Nanoparticles:Â Spectroscopy, Electrochemistry, and Kinetics. Environmental Science & Technology, 2005, 39, 1221-1230.	4.6	865

#	Article	IF	CITATIONS
397	Iron oxide–gold core–shell nanoparticles and thin film assembly. Journal of Materials Chemistry, 2005, 15, 1821.	6.7	211
398	Synthesis, Characterization, and Optical Properties of Pristine and Doped Yttrium Aluminum Garnet Nanopowders. Journal of the American Ceramic Society, 2005, 88, 284-286.	1.9	28
399	Atomic Resolution Imaging of Au Nanocluster Dispersed in TiO2, SrTiO3, and MgO. Journal of the American Ceramic Society, 2005, 88, 3184-3191.	1.9	7
400	Thiophene hydrodesulfurization over nickel phosphide catalysts: effect of the precursor composition and support. Journal of Catalysis, 2005, 231, 300-313.	3.1	313
401	Heteroepitaxial growth and structural analysis of epitaxial α–Fe2O3(1010) on TiO2(001). Journal of Materials Research, 2005, 20, 1250-1256.	1.2	4
402	Potassium chloride nanowire formation inside a microchannel glass array. Applied Physics Letters, 2005, 86, 263110.	1.5	2
403	Changing Morphology of BaO/Al2O3during NO2Uptake and Release. Journal of Physical Chemistry B, 2005, 109, 7339-7344.	1.2	79
404	Distortion of the oxygen sublattice in pure cubic-ZrO2. Journal of Materials Research, 2004, 19, 1315-1319.	1.2	23
405	Effect of Nd ₂ O ₃ Doping on the Densification and Abnormal Grain Growth Behavior of Highâ€Purity Alumina. Journal of the American Ceramic Society, 2004, 87, 378-383.	1.9	24
406	Effects of Template and Precursor Chemistry on Structure and Properties of Mesoporous TiO2Thin Films. Langmuir, 2004, 20, 9095-9102.	1.6	15
407	Anisotropic thermal properties of single-wall-carbon- nanotube-reinforced nanoceramics. Philosophical Magazine Letters, 2004, 84, 419-423.	0.5	32
408	A Direct Route toward Assembly of Nanoparticleâ^'Carbon Nanotube Composite Materials. Langmuir, 2004, 20, 6019-6025.	1.6	158
409	Toward the Solution Synthesis of the Tetrahedral Au20Cluster. Journal of Physical Chemistry B, 2004, 108, 12259-12263.	1.2	106
410	Composition-Controlled Synthesis of Bimetallic Goldâ^'Silver Nanoparticles. Langmuir, 2004, 20, 11240-11246.	1.6	125
411	Physiological indicators of divergent stress responsiveness in male striped bass broodstock. Aquaculture, 2004, 232, 665-678.	1.7	28
412	Interface Structure of an Epitaxial Cubic Ceria Film on Cubic Zirconia. Journal of the American Ceramic Society, 2003, 86, 363-365.	1.9	20
413	Synthesis, Characterization, and Manipulation of Helical SiO2 Nanosprings. Nano Letters, 2003, 3, 577-580.	4.5	198
414	Immobilization of Quantum Dots in the Photo-Cross-Linked Poly(ethylene glycol)-Based Hydrogel. Journal of Physical Chemistry B, 2003, 107, 10464-10469.	1.2	48

#	Article	IF	CITATIONS
415	Temperature-induced phase separation in chromium films. Applied Physics Letters, 2003, 82, 2230-2232.	1.5	11
416	Defect clustering in GaN irradiated with O ⁺ ions. Journal of Materials Research, 2002, 17, 2945-2952.	1.2	46
417	Helical Crystalline SiC/SiO2Coreâ^'Shell Nanowires. Nano Letters, 2002, 2, 941-944.	4.5	252
418	Lithium-Assisted Self-Assembly of Aluminum Carbide Nanowires and Nanoribbons. Nano Letters, 2002, 2, 105-108.	4.5	45
419	The characteristics of interface misfit dislocations for epitaxial α-Fe2O3 on α-Al2O3(0001). Thin Solid Films, 2002, 414, 31-38.	0.8	30
420	X-ray Absorption Near-Edge Structure of Grain-Boundary-Segregated Y and Zr in Creep-Resistant Alumina. Journal of the American Ceramic Society, 2002, 85, 2492-2498.	1.9	18
421	Influence of Dopant Concentration on Creep Properties of Nd ₂ O ₃ â€Doped Alumina. Journal of the American Ceramic Society, 2001, 84, 1010-1016.	1.9	31
422	Fabrication of silicon nitride–Silicon oxynitride in-situ composites. Journal of the European Ceramic Society, 1998, 18, 527-533.	2.8	37
423	Precipitation of carbon nanoparticles encapsulating silicon carbide from molten oxide. Journal of Materials Research, 1998, 13, 2039-2041.	1.2	0
424	Arylaminobenzoate Block of the Cardiac Cyclic AMP-Dependent Chloride Current. Molecular Pharmacology, 1998, 53, 539-546.	1.0	20
425	Microstructure of liquid phase sintered superplastic silicon carbide ceramics. Journal of Materials Research, 1997, 12, 3266-3270.	1.2	25
426	Mechanical properties of green compacts with coated powders. Ceramics International, 1996, 22, 113-117.	2.3	4
427	Structural nano-defects in α-silicon nitride. Journal of the European Ceramic Society, 1996, 16, 679-683.	2.8	5
428	The nature of the defective structure ?-silicon nitride. Journal of Materials Science Letters, 1996, 15, 1805-1807.	0.5	2
429	Dislocation-Related Plasticity of Ceria-Stabilized Zirconia Polycrystals. Journal of the American Ceramic Society, 1996, 79, 1726-1728.	1.9	1
430	Origin of dislocation loops in α-silicon nitride. Journal of Materials Research, 1996, 11, 1725-1732.	1.2	2
431	Effect of chloride channel blockers on the cardiac CFTR chloride and L-type calcium currents. Cardiovascular Research, 1996, 32, 391-399.	1.8	34
432	Fine Structural Features in α-Silicon Nitride Powder Particles and Their Implications. Journal of the American Ceramic Society, 1995, 78, 3393-3396.	1.9	9

#	Article	IF	CITATIONS
433	Vacancy clusters in α-silicon nitride. Philosophical Magazine Letters, 1995, 72, 111-115.	0.5	2
434	Dislocation Loops in a-Silicon Nitride. Journal of the American Ceramic Society, 1993, 76, 2136-2138.	1.9	16
435	Alumina-coating of silicon nitride powder. Journal of the European Ceramic Society, 1992, 10, 83-93.	2.8	54
436	Fracture toughness and acoustic emission in silicon nitride. Journal of Materials Science Letters, 1987, 6, 1459-1462.	0.5	5
437	Imaging Liquid Processes Using Open Cells in the TEM, SEM, and Beyond. , 0, , 56-77.		1
438	Systematic Evaluation of Carbon Hosts for High-Energy Rechargeable Lithium-Metal Batteries. ACS Energy Letters, 0, , 1550-1559.	8.8	20